International Journal of Research
Available at https://edupediapublications.org/journals
e-ISSN: 2348-6848
p-ISSN: 2348-795X
Volume 04 Issue14
November 2017

Power Quality Improvement In Electrical Railway Power System With Fuzzy Based Railway Power Flow Controller

O.Saidulu Reddy
Assistant Professor
Malla Reddy College Of Engineering And Technology

ABSTRACT-*A power factor oriented railway power flow controller (RPFC) for the power quality improvement of ERPS using fuzzy is proposed in this paper. This power can be produced only by a balanced system without current and voltage harmonics. Fuzzy Logic compensation is proposed to diminish the Total Harmonic Distortion (THD) to International standards. Here we are using the fuzzy controller compared to other controllers i.e. The fuzzy controller is the most suitable for the human decision-making mechanism, providing the operation of an electronic system with decisions of experts. The comprehensive relationship of the primary power factor, converter capacity, and the two phase load currents are built in this paper. Besides, as the main contribution of this paper, the optimal compensating strategy suited the random fluctuated two phase loads is analyzed and designed based on a real traction substation, for the purposes of satisfying the power quality standard, enhancing RPFC's control flexibility, and decreasing converter's capacity. Finally, by using the simulation results we can analyze the proposed method.*

Index Terms—Power factor; negative sequence; power quality; power flow controller; electrical railway power system; converter, Fuzzy controller.

INTRODUCTION

Electrical Railway Systems now-a-days becomes more advantages in the fields like transportation, energy saving and environment friendly. Considering the cost-efficiency, the electrical trains are fed by the single phase grid, which are supplied from the three phase to two phase traction transformer in electrical railway power system (ERPS). Due to the random unbalanced two phase loads, amount of negative sequence currents (NSCs) along with the feeder voltage fluctuation in violent are occurred in the utilities and ERPS itself [1], [2]. Besides, though some new generation trains with PWM-based front end rectifier are launched in As the popular PQ improvement rig, static var compensator (SVC) static synchronous compensator (STATCOM) active filter transformer integrated power conditioner [2], railway power flow controller (RPFC) and the well-designed train-mounted front end rectifier are commonly used in ERPS. Passive LC filters were used to eradicate current harmonics by connecting it parallel with the load; these have some disadvantages like, passive filters were not suitable for variable loads, they are premeditated for specific reactive power, and the variation of load impedance can detune the filter However, the high capacity or initial investment slowdown RPFC's industrial application speed. Up to now, few researches have focused on the capacity controlling of RPFC. Benefit from the well-designed LC branches, a novel LC coupled RPFC (LC-RPFC) proposed in [5] can effectively reduce the VA-capacity of its active part, because the dc-link voltage can be reduced about 30%-40% than the conventional RPFC.

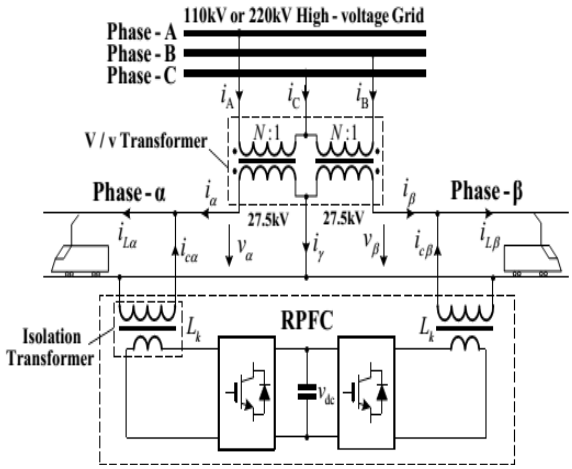

Fig. 1. The typical RPFC integrated two phase ERPS (V/v transformer is adopted as the main transformer).

To further improve RPFC's capacity utilization capability and control flexibility in both designing and operating stages in freight-train dominant ERPS, in this paper, we will focus on the solution of the following aspects:

1) Establishing the relationship between the primary PF with RPFC's compensating capacity; the converter's capacity can be flexibly designed by adjusting the primary PF.

2) In the premise of minimizing RPFC's capacity for a given PF, conceiving an optimal control strategy to decreasing NSC and NSV in a satisfactory level.

3) The proposed control strategy should not only be applied in the simple single phase ERPS, but also in the important common used two phase system (see Fig.1).

International Journal of Research
Available at https://edupediapublications.org/journals
e-ISSN: 2348-6848
p-ISSN: 2348-795X
Volume 04 Issue14
November 2017

GENERAL MATHEMATICAL MODEL OF RPFC INTEGRATED IN TWO PHASE ERPS

First, we define the frame-ABC by the V/v transformer's primary three phase voltage VA, VB, and VC, i.e., Frame-ABC:

$V_A = V_p<0,\quad V_B = V_p<-120, V_C = V_p<-240$ (1)

where V p is the root mean square (RMS) value of VA, VB, and VC.

Reference to Fig. 1, the phasor diagram of the V/v transformer based ERPS can be obtained, as shown in Fig. 2.

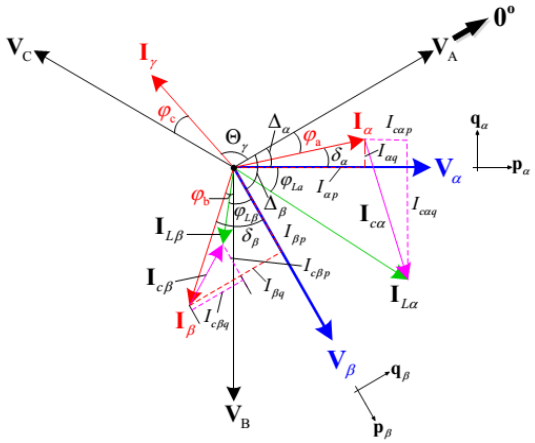

Fig. 2. The phasor diagram of the V/v transformer based ERPC with RPFC.

From Fig. 2, we define the PF in phase-A, B, and C, i.e., PFA~PFC as:

$$PF_A = \cos\varphi_a, PF_B = \cos\varphi_b, PF_A = \cos\varphi_c, \quad (2)$$

where, φk>0 means that the current lags the voltage, otherwise, the current leads the voltage (k=a, b, c). It can be seen from Figs. 1 and 2 that, the output currents Iα and I β of the V/v transformer in frame-pαqα and frame-pβqβ (see Fig.2) can be expressed as

$$\begin{cases} I_\alpha = I_{L\alpha} - I_{C\alpha} = (I_{L\alpha p} - I_{c\alpha p}) + j(I_{L\alpha q} - I_{c\alpha q}) \\ I_\beta = I_{L\beta} - I_{C\beta} = (I_{L\beta p} - I_{c\beta p}) + j(I_{L\beta q} - I_{c\beta q}) \end{cases} \quad (3)$$

where subscript "p" and "q" represents the active and reactive component of the corresponding variable in frame-pαqα or frame-pβqβ, respectively. Additionally, Fig. 2 also shows that the relationship of the p, q components of Iα and Iβ in frame-pαqα and pβqβ satisfy:

$$\begin{cases} I_{\alpha q} = I_{\alpha p}\tan\delta_\alpha = (I_{L\alpha p} - I_{c\alpha p})\tan\delta_\alpha \\ I_{\beta q} = I_{\beta p}\tan\delta_\beta = (I_{L\beta p} - I_{c\beta p})\tan\delta_\beta \end{cases} \quad (4)$$

$$\text{where} \begin{cases} \delta_\alpha = \Delta_\alpha - \varphi_a \\ \delta_\beta = \Delta_\beta - \varphi_b - 120 \end{cases}$$

Note: for V/v transformer, Δα=30° , Δβ=90° [27].

Ignoring the converter's losses, and assuming Vα=Vβ, the active power balance of the back-to-back converter can lead the result of:

$$I_{c\alpha p} = -I_{c\beta P} \quad (5)$$

Based on the Kirchhoff's law, Iα, Iβ, and Iγ in frame-ABC I α ABC , IβABC, and IγABC satisfy

$$-I_\gamma = -I_\gamma^{ABC} = I_\alpha^{ABC} + I_\beta^{ABC} \quad (6)$$

Substituting (3), (4), and (5) into (6), the real and imaginary part of -Iγ, Term-I and Term-II, can be calculated as

$$\begin{cases} Term - I = I_{\alpha p}\cos\Delta_\alpha + I_{\alpha q}\sin\Delta_\alpha \\ \qquad +I_{\beta p}\cos\Delta_\beta + I_{\beta q}\sin\Delta_\beta \\ Term - II = -I_{\alpha p}\sin\Delta_\alpha + I_{\alpha q}\cos\Delta_\alpha \\ \qquad -I_{\beta p}\sin\Delta_\beta + I_{\beta q}\cos\Delta_\beta \end{cases} \quad (7)$$

Substituting (9) into (6), and considering the expressions of Iα p, Iαq, Iβp, and Iβq in (3)-(5), the relationship of Icαp with the two phase load active currents ILαp and ILβp can be calculated as

$$I_{c\alpha p} = \underbrace{\frac{x_1}{x_1+x_1}}_{\mu_\alpha} I_{L\alpha p} - \underbrace{\frac{x_1}{x_1+x_1}}_{\mu_\beta} I_{L\beta p} \quad (8)$$

Re-substituting (10) into (3)-(5), the compensating currents of RPFC can be obtained as

$$\begin{cases} I_{c\alpha p} = \mu_\alpha I_{L\alpha p} - \mu_\beta I_{L\beta P} \\ I_{c\beta p} = -\mu_\alpha I_{L\alpha p} + \mu_\beta I_{L\beta P} \\ I_{c\alpha q} = -[\tan\varphi_{La} + (1-\mu_\alpha)\tan\delta_\alpha]I_{L\alpha p} \\ \qquad -\mu_\beta\tan\delta_\alpha I_{L\beta p} \\ I_{c\beta q} = \mu_\alpha\tan\delta_\beta I_{L\alpha p} - \left[\begin{matrix}\tan\varphi_{L\beta} + \\ (1+\mu_\beta)\tan\delta_\beta\end{matrix}\right] I_{L\beta p} \end{cases} \quad (9)$$

Multiplying the feeder voltage Vα or Vβ in the two sides of (11), RPFC's compensating power in phase α and β, i.e., Pcα, Qcα and Pcβ, Qcβ, can be calculated as

$$\begin{cases} P_{c\alpha} = \mu_\alpha P_{L\alpha} - \mu_\beta P_{L\beta} \\ P_{c\beta} = -\mu_\alpha P_{L\alpha} + \mu_\beta P_{L\beta} \\ Q_{c\alpha} = -[\tan\varphi_{L\alpha} + (1-\mu_\alpha)\tan\delta_\alpha]P_{L\alpha} \\ \qquad -\mu_\beta\tan\delta_\alpha P_{L\beta} \\ Q_{c\beta} = \mu_\alpha\tan\delta_\beta P_{L\alpha} - \left[\begin{matrix}\tan\varphi_{L\beta} + \\ (1+\mu_\beta)\tan\delta_\beta\end{matrix}\right] P_{L\beta} \end{cases} \quad (10)$$

where PLα and PLβ are the load's active power in phase α and β. It can be seen from (12), because Δα, Δβ can be pre-obtained for a certain type of a transformer (e.g., the V/v transformer and other kind of the balance transformers, μα and μβ are only determined by PFA~PFC or φa~φc [see (10) and (2)].

COMPENSATING STRATEGY DESIGN

A. The Possible Compensating Scheme

It can be observed from Fig. 2 that Iα, Iβ, and Iγ (or IA, IB, and IC) may leads or lags VA, VB, and VC, respectively, which means eight (i.e., 8=23) possible combination models with positive or

International Journal of Research
Available at https://edupediapublications.org/journals
e-ISSN: 2348-6848
p-ISSN: 2348-795X
Volume 04 Issue14
November 2017

negative value are existed in φa, φb, and φc. Besides, Fig. 2 also indicates the reactive power of converter-α is larger than the one generated by converter-β (i.e., Icαq>Icβq), to reduce the VA-capacity of converter-α, Iα has to be restricted lagging than VA (i.e., φa>0), so the above eight possible combination models of φa~φc will degenerate into four valuable candidates, which are listed in Table I (i.e., Model-2 to -5).

Table I
Compensating Scheme Of Rpfc

Compensating model	φ_a	φ_b	φ_c
Model-1 (i.e., FCM)	0	0	0
Model-2	>0	<0	>0
Model-3	>0	<0	<0
Model-4	>0	>0	>0
Model-5	>0	>0	<0

* φ_k>0 (or <0) means the inductive (or capacitive) PF (k=a, b, and c)

B. Compensating Capacity Analysis

The VA-capacity SRPFC of the RPFC is:

$$S_{RPFC} = \sqrt{P_{c\alpha}^2 + Q_{c\alpha}^2} + \sqrt{P_{c\beta}^2 + Q_{c\beta}^2} \quad (11)$$

Substituting (12) into (14), the RPFC's VA-capacity in the five compensating model listed in Table I are shown in Fig. 3 It can be seen from Fig. 3(a) that, the VA-capacity of RPFC belongs to five different surfaces in Model-1~5 respectively.

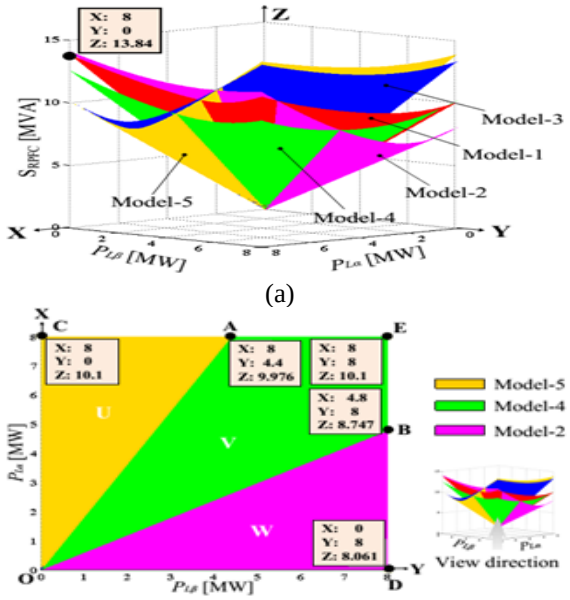

(a)

(b)

Fig. 3. The relationship of SRPFC with the two phase loads' active power in the five valuable compensating models. (a) The surfaces of SRPFC with the two phase loads' active power. (b) The xoy-projection of the surfaces in Fig. 3(a).

Additionally, a surface spliced by the surfaces of Model-2, 4, and 5 has the minimum SRPFC. Compared with Model-1, i.e., FCM, the capacity decreasing ratio of this spliced surface is about 30%, which can make the converter have higher system reliability and efficiency. So, it can be selected as the optimal compensating surface.

If PF*=0.95, from Fig. 3(b) the optimal compensating strategy (OCS) can be preliminary expressed as

$$OCS|_{PF=0.95}: \begin{cases} Model-5, 0MW \le P_{L\beta} < 0.55P_{La} \\ Model-4, 0.55P_{La} \le P_{L\beta} < 1.67P_{La} \\ Model-2, 1.67P_{La} \le P_{L\beta} < 8mw \end{cases} \quad (12)$$

C.The NSC Mitigation Ability Analysis

Excepting of compensating reactive power, mitigation of the NSC is another purpose of RPFC. That is to say, a satisfactory compensating strategy should not only minimize SRPFC, but also has the responsibility to reduce NSC within a satisfactory level.

From (13), (17), and Table I, the relationship of Iunb and PF* of Model-1~ 5 are shown in Fig. 4.

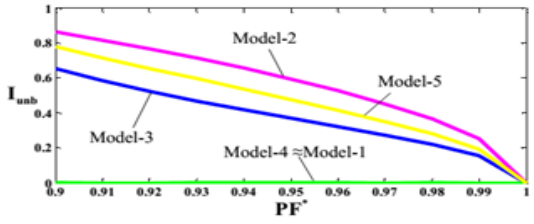

Fig. 4. The curves of Iunb v.s. PF* of Model-1~5.

The compensating strategy combined of Model-2, 4, and 3 has higher comprehensive performance than the one combined by Model-2, 4, and 5.

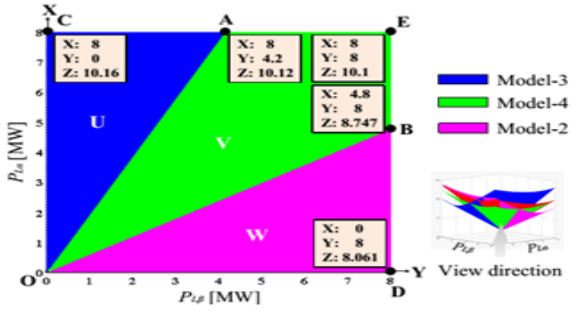

Fig. 5. The optimal compensating strategy of considering the NSC suppressing ability.

So the genuine OCS should be modified from Fig. 3(b) into Fig. 5, and its specification is given in (13).

International Journal of Research
Available at https://edupediapublications.org/journals
e-ISSN: 2348-6848
p-ISSN: 2348-795X
Volume 04 Issue14
November 2017

$$OCS|_{PF=0.95}: \begin{cases} Model-3, 0MW \le P_{L\beta} < 0.415P_{La} \\ Model-4, 0.55P_{La} \le P_{L\beta} < 1.67P_{La} \\ Model-2, 1.67P_{La} \le P_{L\beta} < 8mw \end{cases} \quad (13)$$

Fig. 6 gives the slopes of line OA and OB, i.e., KOA and KOB in different PF* (note: OA and OB are the boundaries of the three compensation model shown in Fig. 5; For implementation of the proposed OCS, a satisfactory performance can also be obtained by fixing KOA on 0.5, and adjusting KOB by PF* according the blue curve shown in Fig. 6. It can be pre-embedded in the digital controller's memory space in practical application.

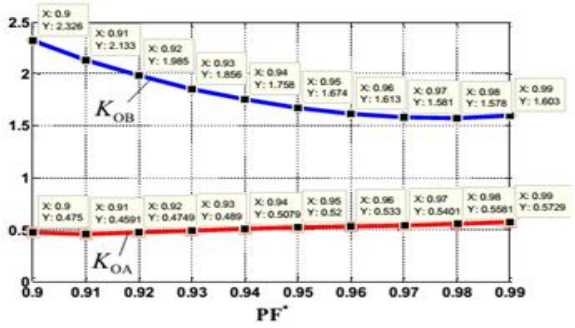

Fig. 6. The curves of slope-AO (i.e., KOA) and BO (i.e., KOB) v.s. PF

C. Negative Sequence Standard Consideration

From (16), the primary NSC I- can be calculated as:

$$I_{-} = \frac{1}{\sqrt{3}N}\sqrt{\xi_1^2 + \xi_2^2}\left(I_{Lap} + I_{L\beta p}\right) \quad (14)$$

The negative sequence capacity S- in the primary side is

$$S_{\infty} = \sqrt{3}V_{sN}I_{\infty} = \sqrt{\xi_1^2 + \xi_2^2}\left(P_{La} + P_{L\beta}\right) = k\left(P_{La} + P_{L\beta}\right) \quad (15)$$

Considering the Chinese national standard of the negative sequence component is

$$V_{unb} = \frac{V_{-}}{V_{+}} = \frac{S_{-}}{S_d} \le \varepsilon_v = 2\% \quad (16)$$

where V - and V+ are the primary negative and positive voltages, Sd is the short circuit capacity of the traction substation.

The negative sequence requirement of the proposed system can be calculated by combining (20) and (21), i.e.,

$$K\left(P_{La} + P_{L\beta}\right) \le S_d * 2\% \quad (17)$$

Fig. 7 gives the two phase loads' distribution chart of a real V/v transformer based traction substation (see Table II).

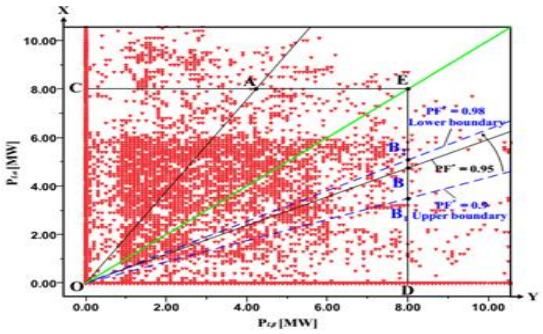

Fig. 7. The two phase load's distribution of a real V/v transformer based traction substation.

The surface of S - vs. PLα and PLβ (within rectangle area of CEDO shown in Fig. 7) can be obtained based on (20) and the Sd given in Table II, which is shown in Fig. 8.

Table II
The Specification Of A Real V/V Transformer

Grid line voltage	110kV
Transformer Capacity	20MVA phase-α: 10MVA phase-β: 10MVA
S_d of the traction substation	486MVA
Short circuit impendence	phase-α and β: 10%
Turn's ratio	110kV:27.5kV

The surface of S - vs. PLα and PLβ (within rectangle area of CEDO shown in Fig. 7) can be obtained based on (20) and the Sd given in Table II, which is shown in Fig. 8. From the shape of the surfaces shown in Fig. 8, it can be concluded that the maximum S - of Model-3, 2, and 4 occurs on the point A, B, and E for any given PF*, respectively.

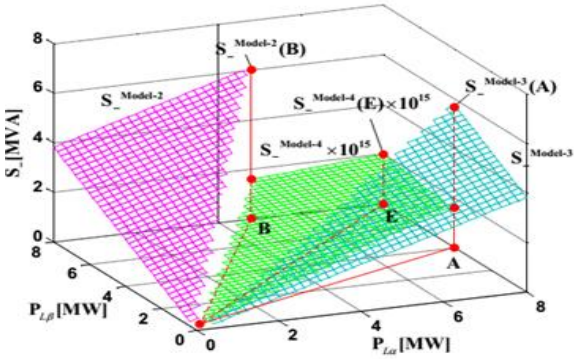

Fig. 8. The relationship of S- with PLα and PLβ (note: PF*=0.95).

Fig. 9 gives the relationship of the S- in A, B, and E, i.e., the maximum S -, S-max, with PF* for this traction substation in Model-2~4. Fig. 9 also

International Journal of Research
Available at https://edupediapublications.org/journals
e-ISSN: 2348-6848
p-ISSN: 2348-795X
Volume 04 Issue14
November 2017

shows that the maximum negative sequence powers controlled by OSC are less than the permission value 9.72MVA.

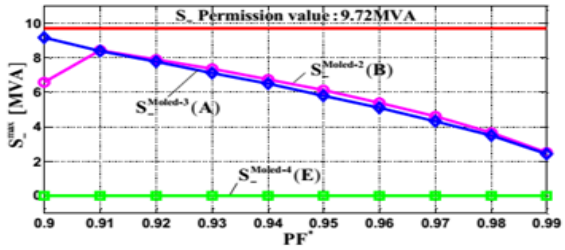

Fig. 9. The relationship of the primary maximum negative capacity with PF* in Modle-2, 3, and 4.

The capacity utilization capability of RPFC should also be included in our concerning scope. Eα in Fig.10 means the maximum converter capacity belongs to converter-α located in point E]. Considering cost-efficiency, PF* can be selected from 0.9 to 0.95 for this traction substation.

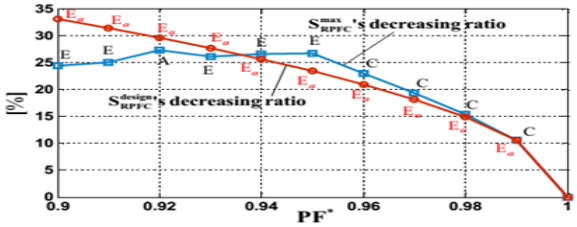

Fig. 10. The relationship of SRPFCmax's reducing ratio [1-maximum SRPFC/FCM based maximum SRPFC] and SRPFCdesign's reducing ratio [1-SRPFCdesign /FCM based SRPFCdesign] with PF* under the control of OCS.

E.Control Strategy Realization

The control system of the RPFC is plotted in Fig. 11. In addition, more attention has to be paid on the realization of the "compensating power calculation" block, and the following four steps can help us to get the target:

1) According the measured two phase loads (e.g., Fig. 7), Sd, and the presented slops of OA and OB shown in Fig. 6, 2) Based on the pre-set PF* (e.g., PF*ϵ[0.9,0.95]), the slopes of OA and OB can be determined from Fig. 6.

3) The compensating model of OCS can be determined by the load point's location in the load distribution panel shown in Fig. 5 or 7, which can be deduced by detecting the two phase loads' active power PLα, PLβ, and the slops of OA and OB pre-obtained in step 2.

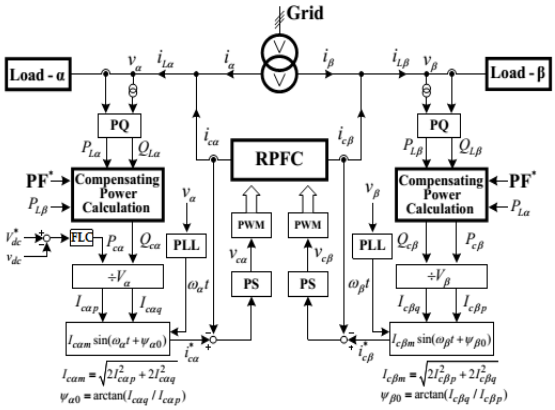

Fig. 11. The control system of the OCS based RPFC.

4) If the compensating model is obtained from step 3, φa, φb, and φc can be calculated from Table I and (13), so as μα and μβ [see (10)]. Hence, the compensating active and reactive power of RPFC can be finally obtained from (12).

III. FUZZY LOGIC CONTROLLER

In FLC, basic control action is determined by a set of linguistic rules. These rules are determined by the system. Since the numerical variables are converted into linguistic variables, mathematical modeling of the system is not required in FC.

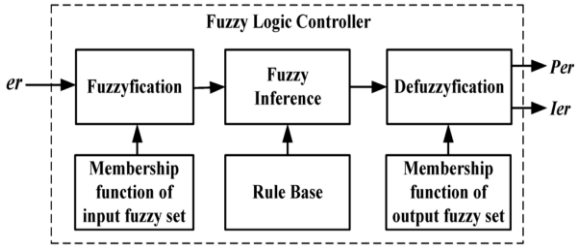

Fig.7.Fuzzy logic controller

The FLC comprises of three parts: fuzzification, interference engine and defuzzification. The FC is characterized as i. seven fuzzy sets for each input and output. ii. Triangular membership functions for simplicity. iii. Fuzzification using continuous universe of discourse. iv. Implication using Mamdani's, 'min' operator. v. Defuzzification using the height method.

TABLE III: Fuzzy Rules

$\frac{e}{\dot{e}}$	NB	NM	NS	ZE	PS	PM	PB
NB	NB	NB	NB	NB	NM	NS	ZE
NM	NB	NB	NB	NM	NS	ZE	PS
NS	NB	NB	NM	NS	ZE	PS	PM
ZE	NB	NM	NS	ZE	PS	PM	PB
PS	NM	NS	ZE	PS	PM	PB	PB
PM	NS	ZE	PS	PM	PB	PB	PB
PB	ZE	PS	PM	PB	PB	PB	PB

Fuzzification: Membership function values are

International Journal of Research
Available at https://edupediapublications.org/journals
e-ISSN: 2348-6848
p-ISSN: 2348-795X
Volume 04 Issue14
November 2017

assigned to the linguistic variables, using seven fuzzy subsets: NB (Negative Big), NM (Negative Medium), NS (Negative Small), ZE (Zero), PS (Positive Small), PM (Positive Medium), and PB (Positive Big). The Partition of fuzzy subsets and the shape of membership CE(k) E(k) function adapt the shape up to appropriate system. The value of input error and change in error are normalized by an input scaling factor.In this system the input scaling factor has been designed such that input values are between -1 and +1. The triangular shape of the membership function of this arrangement presumes that for any particular E(k) input there is only one dominant fuzzy subset. The input error for the FLC is given as

$$E(k) = \frac{P_{ph\,(k)} - P_{ph\,(k-1)}}{V_{ph\,(k)} - V_{ph\,(k-1)}} \quad (12)$$

$$CE(k) = E(k) - E(k\text{-}1) \quad (13)$$

Inference Method: Several composition methods such as Max–Min and Max-Dot have been proposed in the literature. In this paper Min method is used. The output membership function of each rule is given by the minimum operator and maximum operator. Table 1 shows rule base of the FLC.

Defuzzification: As a plant usually requires a non-fuzzy value of control, a defuzzification stage is needed. To compute the output of the FLC height" method is used and the FLC output modifies the control output. Further, the output of FLC controls the switch in the inverter. In UPQC, the active power, reactive power, terminal voltage of the line and capacitor voltage are required to be maintained. In order to control these parameters, they are sensed and compared with the reference values. The set of FC rules are derived from

$$u=-[\alpha E + (1-\alpha)*C] \quad (14)$$

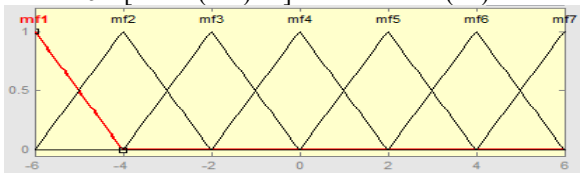

Fig 8 input error as membership functions

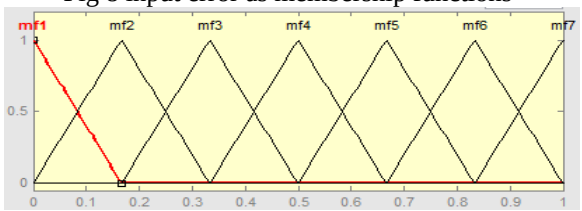

Fig 9 change as error membership functions

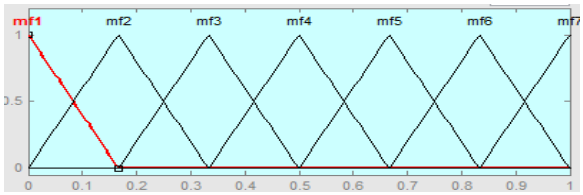

Fig.10 output variable Membership functions

Where α is self-adjustable factor which can regulate the whole operation. E is the error of the system, C is the change in error and u is the control variable.

SIMULATION

To validate the proposed OCS, the simulation model of the studied system shown in Fig. 1 has been established. Figs. 12 and 13 show that, no matter the two phase loads change or not, the primary PF shift along with PF* with the satisfactory performance.

Table III
The Parameters Of The Isolation Transformer And Rpfc

The VA-capacity of IT	5MVA
Short circuit impendence of IT	21%
IT's turn's ratio [a]	27.5kV:27.5kV
The dc-link voltage of RPFC	51.15kV

Table IV
Action Sequence Of The Case Shown In Fig. 12

Time	PF*	Compensation model	Load condition
0.0-0.2s	No RPFC	-	P_{La}=8MW, Q_{La}=6Mvar; $P_{Lβ}$=0MW, $Q_{Lβ}$=0Mvar
0.2-0.4s	0.90	Model-3	
0.4-0.6s	0.95	Model-3	
0.6-0.8s	0.97	Model-3	
0.8-1.0s	1.00	FCM	

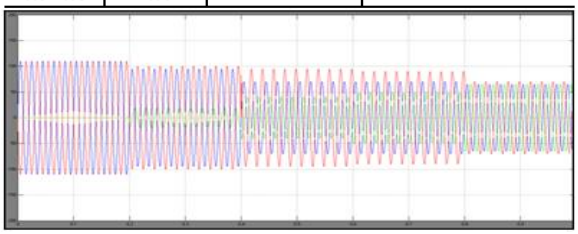

(a)

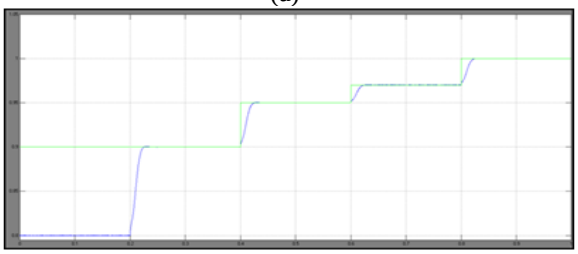

(b)

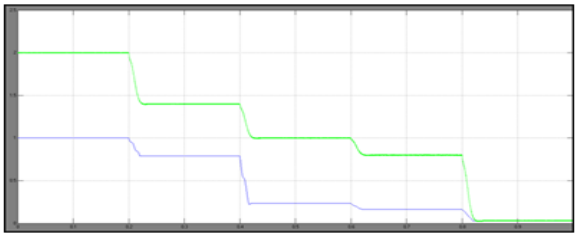

(c)

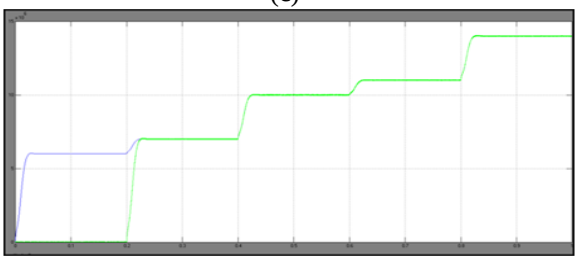

(d)

Fig. 12. The waveforms in the condition of variable PF* with constant load. (a) Primary three phase currents. (b) PF* and PF. (c) Voltage's and current's unbalanced ratio. (d) Capacity of RPFC.

Table V
Action Sequence Of The Case Shown In Fig. 13

Time	Load condition	PF*	Compensation model
0.0-0.2s	P_{La}=0MW, Q_{La}=0Mvar; $P_{Lβ}$=8MW, $Q_{Lβ}$=6Mvar	No RPFC	-
0.2-0.4s	P_{La}=0MW, Q_{La}=0Mvar; $P_{Lβ}$=8MW, $Q_{Lβ}$=6Mvar	1	FCM
0.4-0.6s	P_{La}=8MW, Q_{La}=6Mvar; $P_{Lβ}$=8MW, $Q_{Lβ}$=6Mvar		
0.6-0.8s	P_{La}=8MW, Q_{La}=6Mvar; $P_{Lβ}$=0MW, $Q_{Lβ}$=0Mvar		
0.8-1.0s	P_{La}=0MW, Q_{La}=0Mvar; $P_{Lβ}$=8MW, $Q_{Lβ}$=6Mvar	0.95	Model-2
1.0-1.2s	P_{La}=8MW, Q_{La}=6Mvar; $P_{Lβ}$=8MW, $Q_{Lβ}$=6Mvar		Model-4
1.2-1.4s	P_{La}=8MW, Q_{La}=6Mvar; $P_{Lβ}$=0MW, $Q_{Lβ}$=0Mvar		Model-3

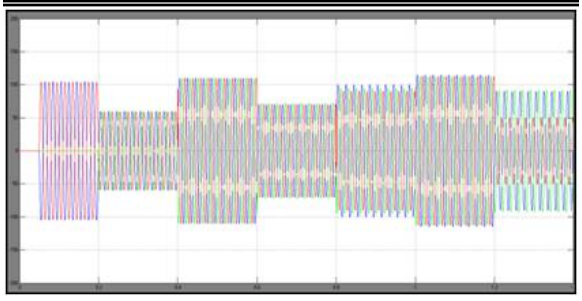

(a)

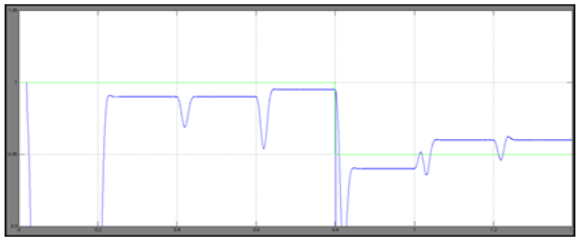

(b)

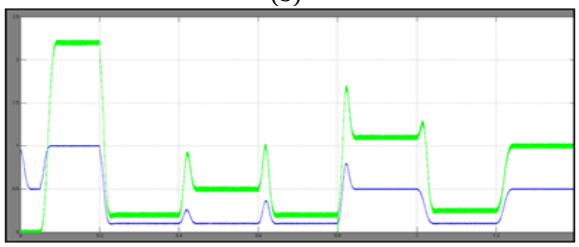

(c)

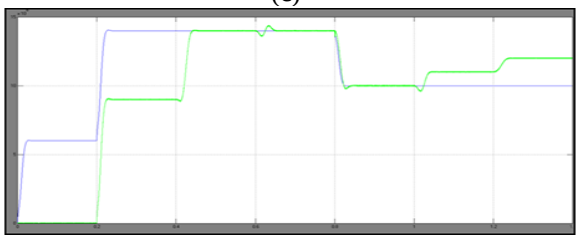

(d)

Fig. 13. The waveforms in the condition of variable load with constant PF*. (a) Primary three phase currents. (b) PF* and PF. (c) Voltage's and current's unbalanced ratio. (d) Capacity of RPFC.

CONCLUSION

A power factor oriented RPFC for the power quality improvement in the common used two phase freight train dominated ERPS is proposed in this paper. The mathematical model of the RPFC integrated ERPS and the comprehensive design method of the proposed control strategy are given in detail, based on a real traction substation. The fuzzy logic controller has several advantages, which are applicable in various fields. In order to improve the better results, FIn the premise of satisfying the standards of the reactive power and NSV, this paper gives an optimal control strategy for the PQ improvement, control flexibility enhancement, and the reduction of RPFC's compensating and designing capacity in two or single phase RPFC integrated ERPS. This technique diminishes the current THD to values consenting to international regulations, and also directs the power factor observed in the point of common coupling between the traction substation and the grid. This control method can make the system have an attractive high cost-efficiency in two or single phase traction load conditions.

REFERENCES

[1] S. Chen, R. Li, and H.4 Hsiang, "Traction system unbalance problemanalysis methodologies," IEEE Trans. Power Del., vol. 19, no. 4, pp. 1877–1883, Oct. 2004.

[2] J. Kilter, T. Sarnet, and T. Kangro, "Modelling of high-speed electrical railway system for transmission network voltage quality analysis: Rail Baltic case study," in Proc. Elect. Power Qual. Supply Reliab. Conf. (PQ), 2014, pp. 323–328.

[3] Z. He, H. Hu, Y. Zhang, and S. Gao, "Harmonic resonance assessment to traction power-supply system considering train model in China high-speed railway," IEEE Trans. Power Del., vol. 29, no. 4, pp. 1735– 1743, Aug. 2014.

[4] G. Raimondo, P. Ladoux, A. Lowinsky, H. Caron, and P. Marino, "Reactive power compensation in railways based on AC boost choppers," IET Electr. Syst. Transp., vol. 2, no. 4, pp. 169–177, Jua. 2012.

[5] Z. Zhang, Y. Li, L. Luo, P. Luo, Y. Cao, Y. Chen et al, "A new railway power flow control system coupled with asymmetric double LC branches," IEEE Trans. Power Electron., vol. 30, no. 10, pp. 5484–5498, Oct. 2015.

[6] S. Gazafrudi, A. Langerudy, E. Fuchs, and K. Al-Haddad, "Power quality issues in railway electrification: a comprehensive perspective," IEEE IEEE Trans. Ind. Electron., vol. 62, no. 5, pp. 3081–3090, May. 2015.

[7] T. Uzuka, "Faster than a speeding Bullet: An overview of Japanese high-speed rail technology and electrification," IEEE Electrification Mag., vol.1, no.1, pp. 11–20, Sep. 2013.

[8] M. Brenna, F. Foiadelli, and D. Zaninelli, "Electromagnetic model of high speed railway lines for power quality studies," IEEE Trans. Power Syst., vol. 25, no. 3, pp. 1301–1308, Aug. 2010.

[9] H. Wang, Y. Liu, K. Yan, Y. Fu, and C. Zhang, "Analysis of static VAr compensators installed in different positions in electric railways," IET Elect. Syst. Transp., vol. 5, no. 3, pp. 129–134, Jan. 2015.

[10] G. Zhu, J. Chen, and X. Liu, "Compensation for the negative-sequence currents of electric railway based on SVC," in Proc. ICIEA. Conf., 2008, pp. 1958–1963.